



1 **The size resolved cloud condensation nuclei (CCN)**  
2 **activity and its prediction based on aerosol**  
3 **hygroscopicity and composition in the Pearl Delta River**  
4 **(PRD) Region during wintertime 2014**

5 Mingfu Cai<sup>1,2</sup>, Haobo Tan<sup>2\*</sup>, Chak K. Chan<sup>3</sup>, Yiming Qin<sup>4,5</sup>, Hanbing Xu<sup>1</sup>, Fei Li<sup>2</sup>,

6 Misha I. Schurman<sup>4</sup>, Liu Li<sup>1</sup>, and Jun Zhao<sup>1\*</sup>

7 <sup>1</sup> School of Atmospheric Sciences, Guangdong Province Key Laboratory for Climate Change and  
8 Natural Disaster Studies, and Institute of Earth Climate and Environment System, Sun Yat-sen  
9 University, Guangzhou, Guangdong 510275, China

10 <sup>2</sup> Institute of Tropical and Marine Meteorology/Guangdong Provincial Key Laboratory of Regional  
11 Numerical Weather Prediction, CMA, Guangzhou 510640, China

12 <sup>3</sup> School of Energy and Environment, City University of Hong Kong, Hong Kong, China

13 <sup>4</sup> Hong Kong University of Science and Technology, Hong Kong, China

14 <sup>5</sup> School of Engineering and Applied Sciences, Harvard University, Cambridge, Massachusetts 02138,  
15 United States

16 \*Corresponding authors: Haobo Tan ([hbtan@grmc.gov.cn](mailto:hbtan@grmc.gov.cn)) and Jun Zhao  
17 ([zhaojun23@mail.sysu.edu.cn](mailto:zhaojun23@mail.sysu.edu.cn))

18

19 **Abstract.** A hygroscopicity-tandem differential mobility analyzer (H-TDMA), a scanning mobility  
20 CCN analyzer (SMCA), and an aerodyne high resolution time-of-flight aerosol mass spectrometer  
21 (HR-ToF-AMS) were used to respectively measure the hygroscopicity, condensation nuclei activation,  
22 and chemical composition of aerosol particles at the Panyu site in the Pearl River Region during  
23 wintertime 2014. The distribution of the size-resolved cloud condensation nuclei (CCN) at four  
24 supersaturations (SS=0.1%, 0.2%, 0.4%, and 0.7%) and the aerosol particle size distribution were  
25 obtained by the SMCA. The hygroscopicity parameter  $\kappa$  ( $\kappa_{\text{CCN}}$ ,  $\kappa_{\text{H-TDMA}}$ , and  $\kappa_{\text{AMS}}$ ) was respectively



1 calculated based upon the SMCA, H-TDMA, and AMS measurements. The results showed that the  
2  $\kappa_{\text{H-TDMA}}$  value was slightly smaller than the  $\kappa_{\text{CCN}}$  one at all diameters and for particles larger than 100  
3 nm the  $\kappa_{\text{AMS}}$  value was significantly smaller than the others ( $\kappa_{\text{CCN}}$ , and  $\kappa_{\text{H-TDMA}}$ ), which could be  
4 attributed to the underestimated hygroscopicity of the organics ( $\kappa_{\text{org}}$ ). The activation ratio (AR)  
5 calculated from the growth factor – probability density function (Gf-PDF) without surface tension  
6 correction was found to be lower than that from the H-TDMA measurement, due most likely to the  
7 uncorrected surface tension ( $\sigma_{\text{s/a}}$ ) that did not consider the surfactant effects of the organic compounds.  
8 We demonstrated that better agreement between the calculated and measured AR could be obtained by  
9 adjusting  $\sigma_{\text{s/a}}$ . Various schemes were proposed to predict the CCN number concentration ( $N_{\text{CCN}}$ ) based  
10 on H-TDMA and AMS measurements. In general, the predicted  $N_{\text{CCN}}$  agreed reasonably well with the  
11 corresponding measured ones using different schemes. For H-TDMA measurements, the  $N_{\text{CCN}}$  value  
12 predicted from the real time AR measurements was slightly smaller (~6.8%) than that from the  
13 activation diameter ( $D_{50}$ ) method due to the assumed internal mixing in the  $D_{50}$  prediction. The  $N_{\text{CCN}}$   
14 values predicted from bulk  $\text{PM}_{10}$  were higher (~11.5%) than those from size-resolved composition  
15 measured by the AMS because a significant fraction of  $\text{PM}_{10}$  was composed of inorganic matter. The  
16  $N_{\text{CCN}}$  calculated from AMS measurement were under-predicted at 0.1% and 0.2% supersaturations,  
17 which could be due to underestimate of  $\kappa_{\text{org}}$  and overestimate of  $\sigma_{\text{s/a}}$ . For  $\text{SS}=0.4\%$  and  $0.7\%$ , slight  
18 over-predicted  $N_{\text{CCN}}$  was found because of the internal mixing assumption. Our results highlight the  
19 need for accurately evaluating the effects of organics on both the hygroscopic parameter  $\kappa$  and the  
20 surface tension  $\sigma$  in order to accurately predict CCN activity.  
21



## 1 1 Introduction

2 Aerosol particles can directly impact global climate by scattering and absorbing solar radiation  
3 (Stocker, 2013), while they can influence cloud formation, life time and optical properties by acting as  
4 cloud condensation nuclei (CCN), indirectly exerting climatic forcing on the Earth's atmosphere. In  
5 general, aerosol particles increase the CCN concentration and hence cause cooling effects on the global  
6 radiation balance. However, to what extent aerosol particles contribute to the radiation forcing is still  
7 highly uncertain (Stocker, 2013). It is hence important to measure chemical composition and properties  
8 of aerosol particles in order to assess their abilities of acting as CCN and contribution to cloud  
9 formation, further facilitating our understanding of the impacts of atmospheric aerosols on regional and  
10 global climate.

11

12 The extent to which aerosol particles can affect cloud formation is dependent on their fraction that can  
13 be activated to become CCN. This fraction of activation is termed as CCN activity that is determined  
14 by the chemical composition, sizes, and the water saturation ratio of the particles (Farmer et al., 2015).

15 The size-dependent saturation ratio (S) can be calculated from the Köhler equation (Köhler, 1936):

$$16 \quad S = a_w \exp\left(\frac{A\sigma_{s/a}M_w}{RT\rho_w D}\right) \quad (1)$$

17 where  $a_w$  is the water activity in solution,  $\sigma_{s/a}$  is surface tension of the solution/air interface,  $M_w$  is  
18 the mole weight of water, R is the universal gas constant, T is temperature in Kelvin, and D is the  
19 diameter of the droplet. The  $a_w$  represents Raoult effect, which means that the activation potential  
20 increases with the concentration of the solution. The term  $\exp\left(\frac{A\sigma_{s/a}M_w}{RT\rho_w D}\right)$  represents Kelvin effect,  
21 which relates the surface curvature to the saturation vapor pressure of the droplet. The activation



1 potential increases with increase of the droplet diameter or decrease of surface tension  $\sigma_{s/a}$  and the  
2  $\sigma_{s/a}$  value is sensitive to the organic surfactant effect. The two important parameters, the water activity  
3 ( $a_w$ ) and surface tension ( $\sigma_{s/a}$ ), are dependent on the composition of the aerosol particles, assuming  
4 those particles have the same properties as their corresponding bulk solutions. The effects of organics  
5 on the CCN activity have been extensively investigated; however, many outstanding questions still  
6 remain. Sorjamaa et al. (2004) suggested that the partitioning of surfactant had to be considered when  
7 evaluating the Kelvin effect and the Raoult effect. According to their experimental results, the  
8 surfactant partitioning could alter the Raoult effect so that the change is large enough to depress CCN  
9 activity. However, another experiment conducted by Engelhart et al. (2008) revealed that the organics  
10 in aged monoterpene aerosols could depress surface tension by about  $0.01 \text{ N m}^{-1}$  and hence increase  
11 CCN activity. Ovadnevaite et al. (2017) also presented observational and theoretical evidences that the  
12 decrease of surface tension could prevail over the Raoult effect, which led to the increase of CCN  
13 activity. Salma et al. (2006) isolated humic-like substances (HULIS) from PM<sub>2.5</sub> fraction aerosol  
14 samples and investigated the surface tension properties of the HULIS pure solutions. Their results  
15 showed that thermodynamic equilibrium on surface could only be reached after several hours. Because  
16 the depression of surface tension was controlled by diffusion of surfactants from the bulk of the droplet  
17 to its surface, the extent of the actual decrease of surface tension was hence kinetically limited. A  
18 hybrid model proposed by Petters and Kreidenweis (2013) was used to predict the effects of surfactants  
19 on the CCN activity. The model predicted strong effects of the surfactants on ternary systems where  
20 common ions were present. However, due to the limited measurement techniques, the available  
21 laboratory data were still not sufficient to support this prediction and more solid data were needed to



1 validate the surfactant effects on the CCN activity.

2

3 The CCN activity can be characterized by the hygroscopicity parameter  $\kappa$  that was initially proposed by

4 Petters and Kreidenweis (2007). Aerosol hygroscopicity represents the ability of the particles to grow

5 by absorbing water vapor from the atmosphere and the extent to which the particles are hygroscopic

6 can be evaluated by the  $\kappa$  values, which can be determined from the H-TDMA or CCNc measurements.

7 The  $\kappa$  values were measured worldwide extensively either in the field measurements or in the

8 laboratory experiments and depending on the organic content of the particles, a wide range of  $\kappa$  values

9 were reported in the literatures. Cerully et al. (2011) showed that the  $\kappa$  values measured in 2007 by

10 Flow-Streamwise Thermal Gradient CCN Chamber (CFSTGC) ranged mostly between 0.1 and 0.4 in a

11 forest environment in Finland. Hong et al. (2014) obtained the average  $\kappa$  values of 0.15 (110 nm) and

12 0.28 (102 nm) measured by H-TDMA at the same site in 2010. Chang et al. (2010) used an AMS to

13 measure aerosol chemical composition and a mole ratio of atomic oxygen to atomic carbon (O/C) at a

14 rural site in Canada. They reported a relationship between the  $\kappa$  values of organics and the O/C ratio as

15  $\kappa_{\text{org}}=(0.29\pm 0.05)*(O/C)$ . Tritscher et al. (2011) conducted smog chamber experiments for

16 measurements of the  $\kappa$  values of aging secondary organic aerosols and they found that the  $\kappa$  was a

17 sensitive indicator of the SOA properties.

18

19 Although the  $\kappa$  values were reported under different environments in many locations, only a few

20 studies were conducted to measure  $\kappa$  in the Pearl River Delta (PRD) region (Cheung et al. 2015;

21 Schurman et al. 2017). Jiang et al. (2016) compared the  $\kappa$  values between wintertime (0.18-0.22) and



1 summertime (0.17-0.21) in Guangzhou. Cai et al. (2017) reported the  $\kappa$  values of about 0.4-0.6 and  
2 0.2-0.3 measured by the H-TDMA respectively in Cape Hedo (Japan) and in Guangzhou (China).  
3 Alternatively, the average  $\kappa$  values can be predicted by the ZSR mixing rule (Zdanovskii, 1948; Stokes  
4 and Robinson, 1966) which is based on the chemical composition of the aerosol particles from the  
5 AMS measurement. Liu et al. (2014) reported the  $\kappa$  values of 0.22 to 0.32 using the ZSR mixing rule,  
6 consistent with the values (0.25 to 0.34) based on the H-TDMA measurement.

7  
8 Once the  $\kappa$  values were determined, they could then be employed to predict the CCN activity that was  
9 characterized by three important parameters: activation diameter ( $D_{50}$ ), CCN number concentration  
10 ( $N_{CCN}$ ), and activation ratio (AR). Until now, the CCN activity (thus the above three parameters) can be  
11 determined using the following three methods:

12 (1) The combination of Cloud Condensation Nuclei counter (CCNc) and Scanning Mobility Particle  
13 Sizer (SMPS). The CCN number was measured by the CCNc at different supersaturation ratios (SS,  
14 typically 0.05% ~ 1%). Meanwhile, the  $D_{50}$  and size-resolved activation ratios could be measured by  
15 combining the CCNc with a differential mobility analyzer (DMA) and a condensation particle counter  
16 (CPC)(Moore et al., 2011; Deng et al., 2011), referred to as Scanning Mobility CCN Analysis (SMCA)  
17 based on measurements from a SMPS (DMA+CPC) and a CCNc. This method can measure the  
18 size-resolved CCN distributions at a high time resolution (Moore et al., 2010) and has been applied in  
19 laboratory experiments (Asaawuku et al., 2009) and field campaign (Moore et al., 2008) to measure  
20 CCN activity.

21 (2) The ZSR method based on chemical composition measurements. The CCN concentrations were



1 inverted from the chemical composition and the size distribution of the aerosol particles measured  
2 respectively from the aerosol mass spectrometer (AMS) and SMPS (Moore et al., 2012; Meng et al.,  
3 2014). The  $\kappa$  was then calculated from the ZSR mixing rule. In general, the particles were assumed to  
4 be internally mixed, which might lead to a large uncertainty (up to 80%) in predicting  $N_{CCN}$  in some  
5 cases (Wang et al., 2010).

6 (3) The H-TDMA method. The size-resolved CCN distribution and activation ratios could be  
7 determined from hygroscopicity and size distribution measured using the H-TDMA (Good et al., 2010;  
8 Wu et al., 2013). The H-TDMA measured the distribution of hygroscopic growth factor (Gf) at a fixed  
9 relative humidity for a selected diameter of aerosol particles. Väisänen et al. (2016) reported that the  
10 measured  $N_{CCN}$  with the H-TDMA agreed well with that from in-cloud prediction, where the sample  
11 was collected from a tower approximately 224 m above the surrounding lake level. On the other hand,  
12 Chan (2008) attributed differences in  $\kappa$  from H-TDMA and CCN measurements to sparingly soluble  
13 organics that did not easily deliquesce in the former measurements.

14  
15 The PRD region is one of the most economically invigorating regions in China. This region is  
16 subjected to severe air pollution due to intense human activities and insufficient pollution control  
17 measures. High particle loading leads to both visibility degradation and large cooling effects due to  
18 decrease of solar radiation. During wintertime, high concentrations of fine particles also cause severe  
19 haze events that pose health risk on human beings at the regional scale. It is hence an ideal location to  
20 investigate the influence of local anthropogenic emissions on the particles properties. However, there is  
21 still lack of understanding on the relationship between the CCN activity and its controlling factors (e.g.,



1 chemical composition and hygroscopicity of aerosol particles), hindering policy-makers to propose  
2 effective measures for air pollution control.  
3  
4 In this study, we used the SMCA, H-TDMA, and HR-ToF-AMS to respectively measure CCN activity,  
5 hygroscopicity and chemical composition. We reported the relationship between CCN activity and  
6 hygroscopicity/chemical composition of aerosol particles in the PRD region, where only a few studies  
7 on such relationship were available in the literature. The measurements were performed during  
8 wintertime 2014 (November and December). The CCN properties were predicted based on the  
9 combined SMCA, H-TDMA and HR-ToF-AMS measurements. The methods employed to predict the  
10 CCN concentrations were evaluated and the impact of organics on CCN concentrations was discussed.

## 11 **2 Experiments and data analysis**

### 12 **2.1 Measurement site**

13 The field measurements were conducted at the Chinese Meteorological Administration (CMA)  
14 Atmospheric Watch Network (CAWNET) Station in Panyu, Guangzhou, China, during wintertime  
15 2014 (November and December). The Panyu Station is located at the center of the PRD region and at  
16 the top of Dazhengang Mountain (23°00'N, 113°21'E) with an altitude of about 150 m. No significant  
17 local emission sources were around the site. Detailed description of the measurement site and  
18 instruments (i.e., the H-TDMA and the AMS) can be found elsewhere (Cai et al., 2017; Qin et al.  
19 2017).

### 20 **2.2 Instrumentation**

#### 21 **2.2.1 Aerosol hygroscopicity measurements**



1 Size-resolved aerosol hygroscopicity and particle number size distribution (PNSD) were measured by a  
2 H-TDMA which was developed by Tan et al. (2013). The hygroscopicity data were only available in  
3 November due to the failure of the H-TDMA during December. An aerosol sampling port equipped  
4 with a  $PM_{1.0}$  impactor inlet was used during the measurement period. Ambient sampling flow first  
5 passed through a Nafion dryer (Model PD-70T-24ss, Perma Pure Inc., USA) to achieve a RH of <10%.  
6 We considered the particles to be dry when the RH values were less than 10%. The particles were  
7 subsequently charged by a neutralizer (Kr85, TSI Inc.) and size-selected by a differential mobility  
8 analyzer (DMA1, Model 3081L, TSI Inc.). The mono-disperse particles with a specific diameter ( $D_0$ )  
9 were then introduced into a Nafion humidifier (Model PD-70T-24ss, Perma Pure Inc., USA) under a  
10 fixed RH of  $(90 \pm 0.44)$  %. Another differential mobility analyzer (DMA2, Model 3081L, TSI Inc.) and  
11 a condensation particle counter (CPC, Model 3772, TSI Inc.) were used to measure the number size  
12 distribution of the humidified particles ( $D_p$ ). Thus, growth factor ( $G_f$ ) of the particles can be  
13 calculated:

$$14 \quad G_f = \frac{D_p}{D_0} \quad (2)$$

15  
16 During the campaign, we selected five dry mobility diameters (40, 80, 110, 150, and 200 nm) for the  
17 H-TDMA measurements. The measurements were performed continuously except for regular  
18 calibration of the instrument. We used standard polystyrene latex spheres and ammonium sulfate to  
19 perform the DMA calibration to ensure the instrument to function normally.

#### 20 **2.2.2 Size-resolved CCN activity measurements**

21 Size-resolved CCN spectra and activation ratios were measured with the SMCA initially proposed by



1 Moore et al. (2010)). In this work, the SMCA consisted of a CCNc-100 (DMT Inc.), a differential  
2 mobility analyzer (DMA, Model 3081L, TSI Inc.) and a condensation particle counter (CPC, Model  
3 3787, TSI Inc.). In the SMCA system, the combined DMA and CPC were used as a scanning mobility  
4 particle sizer (SMPS) during the measurements. The dry particles after the Nafion dryer were  
5 neutralized by the Kr85 neutralizer and were subsequently classified by the DMA. The mono-disperse  
6 particles were split into two streams: one to the CPC for measurement of total particle number  
7 concentration ( $N_{CN}$ ) and another to the CCNc-100 for measurement of the CCN number concentration.  
8 The aerosol and CPC flow rate was both  $1.0 \text{ L min}^{-1}$  for the DMA and the CPC ( $0.5 \text{ L min}^{-1}$  makeup  
9 flow and  $0.5 \text{ L min}^{-1}$  sample flow), respectively. The CCNc-100 drew another aerosol flow rate of  $0.5 \text{ L}$   
10  $\text{min}^{-1}$ . The SMCA was protocoled to measure particles at a mobility diameter range of 10 - 400 nm. The  
11 supersaturation in the CCNc-100 was set to be 0.1%, 0.2%, 0.4% and 0.7% respectively for each  
12 measurement cycle. The CCNc-100 was regularly calibrated with ammonium sulfate particles at the  
13 four SS (0.1%, 0.2%, 0.4%, and 0.7%). Similarly, the DMA was calibrated with standard polystyrene  
14 latex spheres before and after the campaign for quality assurance and control.

### 15 **2.2.3 Aerosol chemical composition measurements**

16 An Aerodyne high-resolution time-of-flight aerosol mass spectrometer (HR-ToF-AMS) was employed  
17 in the campaign to measure non-refractory  $\text{PM}_1$  chemical composition (bulk and size-resolved)  
18 including sulfate, nitrate, ammonium, chloride and organics. The refractory components such as black  
19 carbon, sea salts and crustal species cannot be measured by this instrument. Detailed description of the  
20 HR-ToF-AMS can be found elsewhere (DeCarlo et al., 2006; Jimenez et al., 2003). Here only a brief  
21 description relevant to the measurements is given. The instrument was operated in three modes (pToF,



1 V, and W mode). Particle size distribution could be obtained based on time-of-flight of the particles in  
2 pToF mode. In V and W modes, the resolving power of the mass spectrometer was approximately 2000  
3 and 4000, respectively. The instrument collected alternatively 5-min average mass spectra for the V +  
4 pToF modes and the W mode. The monodisperse pure ammonium nitrate ( $\text{NH}_4\text{NO}_3$ ) particles selected  
5 by a DMA (400 nm) were used weekly in the ionization efficiency (IE) calibration. Background signals  
6 were obtained daily for about 30 minutes by introducing filtered ambient air with a HEPA filter in the  
7 sample flow. Before and after the measurement, the sampling flow rate was calibration with a Gilian  
8 gibrator. We also generated PSL (Duke Scientific) and ammonium nitrate particles in a size range of  
9 178–800 nm to calibrate the pToF size. Note that the mass concentrations were too low for particle  
10 diameters smaller than 65 nm and data for those particles were hence discarded in this study. A more  
11 detailed description of the AMS performance during the measurements can be found in Qin et al. (2017)  
12 and Cai et al. (2017).

13

14 The AMS measured size-resolved chemical composition of particles in vacuum aerodynamic diameter  
15 ( $D_{\text{va}}$ ). It is hence necessary to convert aerodynamic diameter to mobility diameter in order to compare  
16 the AMS data and the SMCA data. We adopted the equation derived by DeCarlo et al. (2004) to do the  
17 conversion. Here we assume a density of  $1700 \text{ kg m}^{-3}$  for particles measured by the AMS (DeCarlo et  
18 al., 2004)

19

## 20 **2.3 Data processing and methodology**

### 21 **2.3.1 Hygroscopicity**



1 Due to the effects of diffusing transfer function, the measured distribution function (MDF) given by  
2 H-TDMA is only a skewed and smoothed integral transform of the actual growth factor probability  
3 density function (Gf-PDF) of the particles (Gysel et al., 2009). Here the TDMAfit algorithm  
4 (Stolzenburg and McMurry, 2008) was applied to narrow the uncertainties caused by the diffusion  
5 broadening. The TMDAfit algorithm describes the Gf-PDF as a combination of several (usually smaller  
6 than three) lognormal distribution functions, in which the parameters of each mode are considered as  
7 mean Gf, standard deviation, and number fraction. The detailed data inversion process of the H-TDMA  
8 instrument can be found in Tan et al. (2013).

9  
10 As mentioned in the introduction, the CCN activity can be represented by a widely used hygroscopicity  
11 parameter  $\kappa$  (Petters and Kreidenweis, 2007). According to the  $\kappa$ -Köhler theory, for a known  
12 temperature,  $\kappa$  and Gf can be related via eq. 3 (Petters and Kreidenweis, 2007):

$$13 \quad \kappa = (Gf^3 - 1) \left[ \frac{1}{RH} \exp\left(\frac{4\sigma_{s/a}M_w}{RTGf\rho_w D} - 1\right) \right] \quad (3)$$

14 where  $\rho_w$  is the density of water (about 998.34 kg m<sup>-3</sup> at 293K),  $M_w$  is the molecular weight of water  
15 (0.018 kg mol<sup>-1</sup>),  $\sigma_{s/a}$  is the surface tension of the solution/air interface and here pure water is  
16 tentatively assumed for the solution ( $\sigma_{s/a}$ =0.0728 N m<sup>-1</sup> at 293K), R is the universal gas constant (about  
17 8.31 J mol<sup>-1</sup>K<sup>-1</sup>), T is thermodynamic temperature in Kelvin, and D is the particle diameter (in meter).

### 18 2.3.2 CCN activation

19 The  $N_{CN}$  and  $N_{CCN}$  data were respectively measured by the SMPS and the CCNc-100 and they were  
20 used to calculate the size-resolved CCN activation ratios (AR) which was defined as the ratio of  $N_{CCN}$   
21 to  $N_{CN}$  at each particle size. The activation ratio can be obtained by fitting the ratio with the sigmoidal



1 function with respect to  $D_p$ :

$$2 \frac{N_{CCN}}{N_{CN}} = \frac{B}{1 + \left(\frac{D_p}{D_{50}}\right)^c} \quad (4)$$

3 where  $D_p$  is the particle dry diameter,  $B$ ,  $D_{50}$  and  $c$  are fitting coefficients that represent the asymptote,

4 the slope, and the inflection point of the sigmoid, respectively (Moore et al., 2010).  $D_{50}$  is also called

5 the critical diameter or the activation diameter, that is, the diameter at which 50% of the particles are

6 activated at a specific SS.

7

8 Alternatively, the hygroscopicity parameter  $\kappa$  can be calculated from the critical saturation ratio ( $Sc$ )

9 and  $D_{50}$  from the following equation (Petters and Kreidenweis, 2007):

$$10 \kappa = \frac{4A^3}{27D_{50}^3(\ln Sc)^2}, \quad A = \frac{4\sigma_s/aM_w}{RT\rho_w} \quad (5)$$

#### 11 2.3.4 CCN prediction based on H-TDMA and AMS measurements

12 The  $N_{CCN}$  can be predicted based on either the aerosol hygroscopicity data (measured by the H-TDMA)

13 or the AMS data. Figure 1 is the schematic diagram we followed to predict  $N_{CCN}$  based on the above

14 two measured datasets. In the first approach, we assumed the critical hygroscopicity parameter  $\kappa_{critical}$  to

15 be a function of the particle diameter and the supersaturation ratio (denoted as  $\kappa_{critical}(D_p, SS)$ ). The

16  $\kappa_{critical}$  was hence defined as the point at which all the particles were activated at a specific diameter and

17 a specific SS. Here we measured hygroscopicity using the H-TDMA at five dry diameters and the CCN

18 concentrations at four SS. We calculated the  $\kappa_{critical}(D_p, SS)$  using eq.5 for a known diameter and SS.

19 The particle with a  $\kappa$  value higher than  $\kappa_{critical}(D_p, SS)$  was considered to be activated as CCN. The

20 activation ratio for a specific diameter at a specific SS was obtained by integrating the  $\kappa$ -PDF for  $\kappa >$

21  $\kappa_{critical}(D_p, SS)$ . The size-resolved activation ratio ( $AR_{SR}$ ) was determined by fitting the  $AR(D_p, SS)$



1 using the eq.4. Thus, the calculated  $N_{CCN}$  can be expressed as:

$$2 \quad N_{CCN}(SS) = \int_0^{\infty} AR_{SR}(Dp, SS)N_{CN}(Dp)dDp \quad (6)$$

3

4 In the second approach, we calculated the  $\kappa$  value according to the ZRS rule based on the AMS

5 measurements:

$$6 \quad \kappa = \sum_i \varepsilon_i \kappa_i \quad (7)$$

7 where  $\varepsilon_i$  is the volume fraction of each component in the particles,  $\kappa_i$  is the  $\kappa$  value of each component.

8

9 The AMS only provided the ion concentrations during the measurements, while the ZSR rule required

10 the volume fraction and hygroscopicity of each component. A simplified ion pairing scheme developed

11 by Gysel et al. (2007) was used to reconstruct the  $NH_4^+$ ,  $SO_4^{2-}$  and  $NO_3^-$  measured by the AMS:

$$n_{NH_4NO_3} = n_{NO_3^-}$$

$$n_{H_2SO_4} = \max(0, N_{SO_4^{2-}} - n_{NH_4^+} + n_{NO_3^-})$$

$$n_{NH_4HSO_4} = \min(2n_{SO_4^{2-}} - n_{NH_4^+} + n_{NO_3^-}, n_{NH_4^+} - n_{NO_3^-})$$

$$n_{(NH_4)_2SO_4} = \max(n_{NH_4^+} - n_{NO_3^-} - n_{SO_4^{2-}}, 0)$$

$$12 \quad n_{HNO_3} = 0, \quad (8)$$

13 where  $n$  denotes the number of moles of each component (i.e.,  $NH_4^+$ ,  $SO_4^{2-}$  and  $NO_3^-$ ). Here we used

14 the ADDEM proposed by Topping et al.(2005) to calculate the  $\kappa$  values of the inorganic species and

15 those of the organics were tentatively assumed to be 0.1 (Meng et al., 2014). Table 1 lists the  $\kappa$  values

16 of the relevant species used in the study based on the calculations and the above assumption.

17



1 The  $D_{50}$  can be calculated from the above  $\kappa$  values using eq.4. The CCN concentration is obtained by  
2 integrating the cloud nuclei concentration for particles larger than  $D_{50}$  based on the particle size  
3 distribution:

$$4 \quad N_{CCN}(SS) = \int_{D_{50}}^{\infty} N_{CN}(Dp) dDp \quad (9)$$

5

### 6 **3. Results and discussion**

#### 7 **3.1 Overview**

8 Table 2 summarizes the observed CCN activity during the campaign. Overall, the average  $N_{CCN}$  at 0.1,  
9 0.2, 0.4, and 0.7% SS were about 3100, 5100, 6500, and 7900  $\text{cm}^{-3}$ , respectively. The average  
10 activation ratios (AR) at the above four SS were 0.26, 0.41, 0.53 and 0.64, respectively. The average  
11  $D_{50}$  at the above four SS were 156, 107, 78 and 58 nm, respectively. The  $N_{CCN}$  at 0.7% SS was  
12 respectively lower than those of the previous measurements (10731  $\text{cm}^{-3}$  at 0.67% SS) in July 2006 in  
13 Guangzhou (Rose et al., 2010), but much higher than those measured (2085  $\text{cm}^{-3}$  at 0.7% SS) in May  
14 2011 in Hong Kong (Meng et al., 2014), while the AR was lower than those from the previous  
15 measurements in Guangzhou (0.59 at 0.67% SS, Rose et al., 2010) and similar to those from the  
16 measurements in Hong Kong (0.64 at 0.7% SS, Meng et al., 2014). The  $D_{50}$  was larger than that in the  
17 previous measurements in Guangzhou (49 nm) and in Hong Kong (47 nm), due to the lower particle  
18 hygroscopicity in Guangzhou. The differences of the  $\kappa_{CCN}$  values between the two measurements (0.21  
19 in this winter campaign vs 0.28 during the summer season in Guangzhou both at 0.7% SS) suggested  
20 that the particles in the summer were in general more hygroscopic and hence were more readily  
21 activated than those in the winter, implying different chemical composition of the particles between the



1 two distinct seasons.

2

3 Figure 2 shows the average mass fraction of NR-PM<sub>1</sub> bulk composition and size-resolved (64-731 nm)

4 composition. The organics was dominant in the bulk NR-PM<sub>1</sub> (50%), followed by sulfate (26%) and

5 nitrate (12%) (Fig.2a). The mass fraction of the organics decreased with the size (Fig. 2b), from 69% at

6 64 nm to 42% at 397 nm. The mass fraction of organics at 397 nm was close to that of NR-PM<sub>1</sub> bulk,

7 due to the fact that the PM<sub>1</sub> mass is dominated by particles in a diameter range of 200~500 nm (Tan et

8 al., 2016). Aerosol particles with larger sizes were more readily exposed to complex atmospheric

9 composition during their aging process, contributing from partitioning between gas phase and particle

10 phase via photochemical reactions, surface heterogeneous reactions etc. In comparison, the dominant

11 NR-PM<sub>1</sub> species observed in Hong Kong were sulfate (51.0%) and organics (28.2%) (Lee et al., 2013),

12 significantly different from our measurements, due probably to different origins of the dominant air

13 masses between the two seasons. The measurement site in Guangzhou was impacted predominantly by

14 the air mass from north, where straw burning contributes to a high mass fraction of organics matter

15 (Cao et al., 2008).

16

17 Figure 3 shows the  $\kappa$  values based respectively on the CCN ( $\kappa_{\text{CCN}}$ ), AMS ( $\kappa_{\text{AMS}}$ ), and H-TDMA

18 ( $\kappa_{\text{H-TDMA}}$ ) measurements, along with the measured particle number size distribution (PNSD, 10-400 nm)

19 during the campaign. The shadow area represents the interquartile range of the PNSD. A distinct peak

20 at around 90 nm was observed from the PNSD (Fig. 3). The  $\kappa_{\text{AMS}}$  was calculated based on the

21 size-resolved chemical composition, assuming the particles are internally mixed. At 0.7% SS, the D<sub>50</sub>



1 was about 58 nm. Hence no  $\kappa_{\text{AMS}}$  was reported at this SS since we only measured particle composition  
2 above 63 nm using the AMS in this study. The  $\kappa$  values were shown in the interquartile range, with the  
3 largest variation from the CCN measurements (Fig. 3). Figure 3 showed that the  $\kappa_{\text{H-TDMA}}$  values were  
4 lower than those of the corresponding  $\kappa_{\text{CCN}}$  at most of the SS, consistent with the previous observation  
5 (Pajunoja et al., 2015). This was probably due to the facts that particles contain a certain fraction of low  
6 solubility composition, such as secondary organic aerosols (SOA), contributing differently to  
7 hygroscopic growth and CCN activation. The available AMS data (Fig. 3) show that the  $\kappa_{\text{AMS}}$  values  
8 were lower than the corresponding  $\kappa_{\text{CCN}}$  and  $\kappa_{\text{H-TDMA}}$  values at all size ranges and the differences  
9 become larger with increasing particle sizes. This was probably due to underestimated hygroscopicity  
10 in the organic composition when using the AMS data, since we assumed a  $\kappa$  value of 0.1 for all  
11 organics at all particle sizes. The hygroscopicity increased with particle diameters due to aerosol aging  
12 which increased the hygroscopic organic contents. The measured  $\kappa_{\text{mean}}$  values fall in a range of  
13 0.22-0.30 for the particle sizes of 40-200 nm measured by H-TDMA in this study. The other aerosol  
14 hygroscopicity measurement in PRD (Jiang et al., 2016) reported the  $\kappa_{\text{mean}}$  values ranging from 0.18 to  
15 0.22 in 2012 winter season and 0.17 to 0.21 in 2013 summer season, suggesting an increase of the  
16 aerosol hygroscopicity which might result from an increasing mass fraction of nitrate in recent years  
17 (Zhang et al., 2015; Itahashi et al., 2018).

18

19 Figure 4 shows the activation ratios (AR) measured by SMCA at four supersaturation ratios (0.1, 0.2,  
20 0.4, 0.7%) for particles below 300 nm. The activation curves obtained in this study were segmented  
21 into three sections: a steady rise at low ARs, a middle sharp increase, and a plateau at almost 100% AR.



1 We defined the steepness as the rate at which the AR increased with the particle sizes. Figure 4 shows  
2 the steepness increased with the SS, indicating that the curves became steeper with the SS and a larger  
3 variation of the  $D_{50}$  was expected. In addition, the CCN activity was more sensitive to particle  
4 diameters at higher SS, which can be seen from partial derivative of  $\kappa_{critical}$  by  $\partial D_{50}$  (eq. 5):

$$5 \quad \frac{\partial \kappa_{critical}}{\partial D_{50}} = -\frac{4A^3}{9D_{50}^4(\ln Sc)^2} \quad (10)$$

6  
7 For a certain SS, the  $\kappa_{critical}$  value became more sensitive to  $D_{50}$  with decrease of the  $D_{50}$ .  
8 Meanwhile, a high SS usually led to a low  $D_{50}$ . Therefore, the AR would vary with  $D_p$  more readily at  
9 higher SS and the curve would become steeper. A higher SS allowed a smaller particle to be activated  
10 and the activation curve became steeper, and vice versa for a lower SS.

11  
12 The steepness of activation curve was also associated with the heterogeneity of aerosol chemical  
13 composition, that was, a steeper activation curve meant that aerosol particles had higher similarity in  
14 hygroscopicity. A bimodal distribution (peaks at about 1-1.1, and 1.5-1.7 Gf) of the Gf-PDFs was  
15 observed along the Gf coordinate at all the five sizes of the particles measured by H-TDMA in this  
16 study (Fig. 5), corresponding respectively to the less- and more-hygroscopic modes. The peak in the  
17 less-hygroscopic mode declined and was shifted to smaller Gf, while the one in the more-hygroscopic  
18 mode climbed and shifted to larger Gf with increase of the diameter of the particle, indicating larger  
19 particles tend to be internally mixed. Here a parameter  $\sigma$  is introduced to illustrate the deviation of  
20 Gf-PDF (Gysel et al., 2009):

$$21 \quad Gf_{mean} = \int_0^{\infty} Gf c(Gf) dGf \quad (11-1)$$



$$\sigma = \left( \int_0^{\infty} (Gf - Gf_{mean})^2 c(Gf) dGf \right)^{\frac{1}{2}} \quad (11-2)$$

2 where the  $c(Gf)$  denotes Gf-PDF and  $Gf_{mean}$  denotes number weighted mean  $Gf$ . The  $\sigma$  was  
3 employed as a measure of the spread of Gf-PDF which represents the heterogeneity of aerosol chemical  
4 composition (Sjogren et al., 2008; Liu et al., 2011). A small  $\sigma$  indicated that the heterogeneity of  
5 aerosol chemical composition was low and aerosol particles had higher similarity in hygroscopicity.  
6 The parameter  $C$  determined the shape of activation curve which was segmented into steep and  
7 smooth parts. A small  $C$  value means a steep activation curve and vice versa. Here an activation curve  
8 was assumed to be steep when the  $C$  values are lower than the lower quartile of all the  $C$  values,  
9 while the activation curve was considered to be smooth when the  $C$  values are higher than the upper  
10 quartile of all the  $C$  values. Table 3 summarizes the  $\sigma$  values of GF-PDF for the corresponding steep  
11 and smooth activation curve at the four supersaturations. In general, the  $\sigma$  increased with the diameter,  
12 indicating that larger particles had higher heterogeneity of aerosol chemical composition. Meanwhile,  
13 the  $\sigma$  values for smooth curve were generally higher than the  $\sigma$  values for steep curve. The results  
14 implied that the shapes of activation curves were related to the heterogeneity of aerosol chemical  
15 composition.

### 16 **3.2 Impact of organics on CCN activity**

17 Figure 6 shows the relationship between the  $D_{50}$  obtained from the SMCA measurements and the  
18 size-resolved mass fractions of organics ( $f_{org}$ ) at three supersaturation ratios (0.1%, 0.2%, and 0.4% SS).  
19 In general, the  $D_{50}$  increased with  $f_{org}$  at the three SS, with a slope of 127, 667, 21, and a fitting  
20 coefficient ( $R^2$ ) of 0.47, 0.31, 0.1 at 0.1%, 0.2%, and 0.4% SS, respectively. The particles usually  
21 became less hygroscopic with increase of the organic fractions ( $f_{org}$ ), which then required larger



1 particles to be activated. At lower SS, better correlations were found between the  $f_{org}$  and the  $D_{50}$   
2 because the  $D_{50}$  was more sensitive to hygroscopicity (The activation ratios increase more slowly with  
3 particle sizes at lower SS as shown in Fig. 4). It was hence more obvious at lower SS that the  
4 modification of the particle hygroscopicity caused by the change of the mass fraction of organics  
5 matter could greatly modify the  $D_{50}$  which might further affect the CCN activity. At higher SS,  
6 according to eq. 5, particles were more easily activated as CCN and the change of particles  
7 hygroscopicity would not significantly alter the CCN activity.

8  
9 Organics can affect the CCN activity via two opposite ways: they can decrease the CCN activity by  
10 increasing the less hygroscopic organic fraction of the particles and thus increase the  $D_{50}$  as shown in  
11 Fig. 6; they can also increase the CCN activity by decreasing the surface tension of the particles. The  
12 latter effect has been demonstrated experimentally. For example, an increase of CCN activity was  
13 observed when organics were added to sulfate ammonium (Engelhart et al., 2008). In this study, we  
14 investigated the impacts of organics on CCN activity through adjusting the value of surface tension  
15 until the calculated AR values based on H-TDMA measurements agree with those obtained from  
16 SMCA measurements (measured AR). As shown in Fig. 7, the calculated AR values were  
17 systematically lower than the corresponding measured ones if the surface tension of bulk pure water  
18 ( $0.072 \text{ N m}^{-1}$ ) was assumed when calculating the AR from the H-TDMA measurements.

19  
20 The surface tension of a nanoparticle was substantially different from that of its bulk solution due to the  
21 curvature effect. The effects of size and composition on the surface tension were currently not well



1 understood. Here we proposed an approach to evaluate the impact of organics on the surface tension  
2 ( $\sigma_{s/a}$ ) based on the fraction change of the calculated AR to the measured AR. We defined this fraction  
3 change ( $\delta_{AR}$ ) as a function of surface tension, diameter, and supersaturation:

$$4 \quad \delta_{AR}(\sigma_{s/a}, Dp, SS) = \frac{AR_m(Dp, SS) - AR_c(\sigma_{s/a}, Dp, SS)}{AR_m(Dp, SS)} \times 100\% \quad (12)$$

5 where  $AR_m(Dp, SS)$  is the measured AR for a certain diameter and SS,  $AR_c(\sigma_{s/a}, Dp, SS)$  is the  
6 calculated AR for a certain diameter, SS, and  $\sigma_{s/a}$ . We excluded particles at the size of 200 nm because  
7 they were easily activated even at 0.1% SS and the  $\delta_{AR}$  was expected to be independent of  $\sigma_{s/a}$ . Here the  
8  $\sigma_{s/a}$  value varied between 0.03 and 0.072 N m<sup>-1</sup> (surface tension of pure water). Figure 8 shows the  $\delta_{AR}$   
9 as a function of  $\sigma_{s/a}$  for the four particle diameters (40, 80, 110, 150 nm). The  $\delta_{AR}$  decreased with  
10 increase of the  $\sigma_{s/a}$  for all given particle sizes, changing more rapidly for smaller particles (i.e., from  
11 200% to -100% for 40 nm) than bigger particles (i.e., from 20% to -10% for 150 nm). The R<sup>2</sup> between  
12 measured AR and predicted AR for a certain diameter and four supersaturations at  $\sigma_{s/a}=0.072$  N m<sup>-1</sup>  
13 were 0.35, 0.93, 0.95 and 0.91, respectively. The  $\delta_{AR}$  values reached zero when the  $\sigma_{s/a}$  was set to be  
14 about 0.054 N m<sup>-1</sup> for 40, 80, and 110 nm particles, and 0.062 N m<sup>-1</sup> for 150 nm particles, with a R<sup>2</sup> of  
15 0.88, 0.94, 0.94 and 0.88 respectively. As a compromise, here we adopt a  $\sigma_{s/a}$  value of 0.058 N m<sup>-1</sup>  
16 (denoted as  $\sigma_{s/a}^*$ ) to predict AR. This  $\sigma_{s/a}^*$  value increased significantly the R<sup>2</sup> compared to that based  
17 on pure water assumption (0.072 N m<sup>-1</sup>) for 40 nm particles, while it was reasonable well for other  
18 sizes of particles (80, 110, 150 nm). The AR was then recalculated using the  $\sigma_{s/a}^*$  value and the  
19 prediction was significantly improved (Fig. 9). The results demonstrated that partitioning of organics  
20 into aerosol particles would decrease their surface tension. Therefore, the pure water assumption for  
21 surface tension would lead to high uncertainties when it applied to predict the activation ratios of the



1 aerosol particles at a certain size. Note that we did not consider the effects of individual organics due to  
2 the limited data from the chemical composition measurements. How chemical composition affects the  
3 surface tension of the particles is yet to be investigated.

### 4 **3.3 The $N_{CCN}$ prediction**

#### 5 **3.3.1 The $N_{CCN}$ prediction based on the H-TDMA measurements**

6 In this study, we used several approaches to predict the  $N_{CCN}$  based on the H-TDMA measurements,  
7 from either the activation curve or the  $D_{50}$ . Table 4 summarizes the methods that were used to predict  
8 the  $N_{CCN}$ , along with the slope and  $R^2$  between the predicted and the measured values. The mixing state  
9 of the aerosol particles is an important parameter in determining the  $N_{CCN}$ . The activation curve  
10 represented actual mixing state, while the  $D_{50}$  approach assumed that all particles were internally mixed.  
11 Scheme 5 in Table 4 was the method based on the activation curve with the new  $\sigma_{s/a}^*$  ( $0.058 \text{ N m}^{-1}$ ). Eq.  
12 6 and Eq. 9 were respectively used to calculate the  $N_{CCN}$  following scheme 1, 2, 5, and the rest of the  
13 schemes. Scheme 5 (real time activation curve using  $\sigma_{s/a}^*$ ) provided the best  $N_{CCN}$  predicted value  
14 (closest to the measured one), followed by scheme 3 (real time  $D_{50}$ ) > scheme 4 (average  $D_{50}$ ) >  
15 scheme 1 (real time activation curve) > scheme 2 (average activation curve). The  $R^2$  values for all the  
16 approaches were in general high (around 0.93). The CCN prediction based on scheme 2 led to the  
17 largest underestimation over the measured values. In general, the real time data (scheme 1 and 3) gave  
18 better predicted  $N_{CCN}$  than the corresponding average data (schemes 2 and 4).

19

20 Figure 10 shows the correlation between the measured  $N_{CCN}$  and the predicted  $N_{CCN}$  from scheme 1-5  
21 at the four SS. For scheme 1-4, the predicted  $N_{CCN}$  values were found to be the largest deviation from



1 the corresponding measured ones at 0.1% SS among all the approaches, probably due to the pure water  
2 assumption for surface tension ( $\sigma_{s/a} = 0.072 \text{ N m}^{-1}$ ). Meanwhile, because the CCN activity was sensitive  
3 to hygroscopicity of the particles at low SS, the uncertainties of hygroscopicity data would lead to large  
4 errors in the prediction of CCN. As discussed in the previous section, the  $D_{50}$  was more sensitive to the  
5  $\sigma_{s/a}$  at lower supersaturations, leading to a large deviation of the  $N_{\text{CCN}}$  from the measured value. The  
6 best agreement between the calculated AR and the measured AR was seen using scheme 5 as the slopes  
7 at the four SS were close to 1 (Fig. 10, q-t).

8

### 9 3.3.2 The $N_{\text{CCN}}$ prediction based on AMS measurements

10 We proposed five approaches based on H-TDMA measurements to predict the  $N_{\text{CCN}}$  in the previous  
11 section. Alternatively, we can calculate the  $N_{\text{CCN}}$  based on AMS measurements. Here we proposed four  
12 methods based on either size-resolved chemical composition or bulk  $\text{PM}_{10}$  chemical composition from  
13 the AMS measurements (Table 5). Here we assumed that the particles were internally mixed and the  
14 median  $\kappa_{\text{AMS}}$  obtained from bulk composition was 0.28, higher than those from size-resolved  
15 composition (0.24-0.26 in Fig. 3), probably due to a higher mass fraction of inorganic matters in bulk  
16 NR- $\text{PM}_{10}$  (Fig. 2). We excluded the size-resolved data at 0.7% SS due to their poor quality. Figure 11  
17 shows the correlation between the measured and predicted  $N_{\text{CCN}}$  from schemes 6-9. The  $N_{\text{CCN}}$  was  
18 under-predicted at 0.1% SS and was over-predicted at 0.7% SS. We proposed three potential factors  
19 that might impact  $N_{\text{CCN}}$  prediction based on AMS measurements. (1) The assumed  $\kappa_{\text{org}}$  values were  
20 probably underestimated for particles larger than 100 nm, leading to the underestimated  $N_{\text{CCN}}$  at low SS.  
21 As shown in Fig. 3, the predicted  $\kappa$  shows a larger deviation from the measured value for a larger



1 particle. The  $D_{50}$  values were more sensitive to particle hygroscopicity at lower SS as discussed in the  
2 previous section. (2) The pure water assumption for surface tension. As we have shown in the previous  
3 section, the  $\sigma_{s/a}$  values for the aerosol particles were found to be much smaller than the  $\sigma_{s/a}$  for pure  
4 water ( $0.072 \text{ N m}^{-1}$ ). As a result, the pure water assumption for surface tension led to the  $N_{CCN}$   
5 underestimation. In addition, again the  $D_{50}$  was more sensitive to  $\sigma_{s/a}$  at the low SS. (3) The exclusion  
6 of black carbon (BC) particles and the mixing state assumption. The BC particles were known to be  
7 non-hygroscopic and had a low CCN activity. During the campaign period, the average BC  
8 concentration was about  $5.91 \mu\text{g}/\text{m}^3$  which accounts for 7 % in  $\text{PM}_{2.5}$ . The assumption of no BC  
9 particles would lead to the overestimation of  $N_{CCN}$ . The assumption of particles being internally mixed  
10 in the AMS measurements would lead to an overestimation of the  $N_{CCN}$  when the ambient particles tend  
11 to be externally mixed (Wang et al., 2010; Sánchez Gácita et al., 2017). However, the internal mixing  
12 assumption seems to play a minor role in predicting the  $N_{CCN}$  at 0.1% SS since the particles at about  
13 140-180 nm tend to be internally mixed as shown in Fig. 5. In this case, the  $\kappa_{\text{org}}$  assumption and the  
14 pure water assumption played more important roles than the mixing state assumption at low SS (i.e.,  
15 0.1% SS). Figure 11 shows significant  $N_{CCN}$  underestimation at 0.1% SS (panels a, e, i, m), while more  
16 or less comparable to the measured  $N_{CCN}$  at higher SS (i.e. 0.2%, 0.4%, 0.7%). The difference between  
17 the  $\kappa_{\text{AMS}}$  and  $\kappa_{\text{CCN}}$  became smaller and the corresponding  $D_{50}$  value decreased with the increase of the  
18 SS so that the impacts of the  $\kappa_{\text{org}}$  assumption and the pure water assumption became minor with the  
19 increase of the SS. Instead, the internal mixing state assumption would play a more important role in  
20 the prediction (Meng et al. 2014). As shown in Fig. 5, the peak height and area of the less-hygroscopic  
21 mode became larger for the smaller size particles (i.e. 40 nm particles), implying that small particles



1 were likely to be externally mixed, that is, the non or less hygroscopic species including BC and  
2 insoluble organics were less likely coated with inorganics salts. Hence the internal mixing assumption  
3 could lead to an overestimated  $N_{CCN}$ .  
4  
5 As discussed above, the two important parameters ( $\kappa_{org}$  and  $\sigma_{s/a}$ ) had significant impacts on the  $N_{CCN}$   
6 prediction. We denoted  $\kappa_{org}^*$  and  $\sigma_{s/a}^*$  as important representations respectively for hygroscopicity and  
7 surface tension contributed from organics. We also pointed out that the  $\kappa_{org}$  was dependent on the  
8 particle size and hence here we further assumed the  $\kappa_{org}^*$  values to be 0.15 and 0.1 respectively for  
9 particles larger and smaller than 100 nm. Note that we previously assumed the  $\kappa_{org}$  to be 0.1 for all  
10 particle sizes. Here we gave an example of the improvements at 0.1% SS when the  $\kappa_{org}$  and  $\sigma_{s/a}$  values  
11 were respectively replaced with the  $\kappa_{org}^*$  and  $\sigma_{s/a}^*$  ones (Fig. 12). The  $\kappa_{AMS}$  value calculated at 0.1% SS  
12 based on  $\kappa_{org}^*$  was 0.288, very close to the corresponding  $\kappa_{CCN}$  value (0.30), indicating that an  
13 improvement was made for the  $N_{CCN}$  prediction when including the  $\kappa_{org}^*$  value. The  $N_{CCN}$  prediction  
14 could be greatly improved when include both  $\sigma_{s/a}^*$  and  $\kappa_{org}^*$  in the calculation (i.e, from 44% in Fig. 11a  
15 to 4% in Fig. 12b). In addition, we also investigated the effects of the  $\sigma_{s/a}$  values in a range of 0.054 to  
16 0.062 N m<sup>-1</sup> as discussed in section 3.2. The shadow area in Fig. 12b represents the variation of linear  
17 fit between the measured and predicted  $N_{CCN}$ . An under- and over-estimated value of 16% (slope=0.84)  
18 and 8% (slope=1.08) was obtained for the predicted  $N_{CCN}$  to the measured  $N_{CCN}$  using a  $\sigma_{s/a}$  value of  
19 0.054 and 0.062 N m<sup>-1</sup> respectively, indicating that the predicted  $N_{CCN}$  agreed reasonably with the  
20 measured ones when the  $\sigma_{s/a}$  values between 0.054 and 0.062 N m<sup>-1</sup> were used in this study. We  
21 conclude that the predicted  $N_{CCN}$  can agree better with the measured one when including both  $\sigma_{s/a}^*$  and



1  $\kappa_{\text{org}}^*$  in the calculation at low SS.

2

### 3 **4 Summary and Conclusions**

4 The CCN activity is an important parameter that determines the extent to which atmospheric particles  
5 can influence cloud formation. It is hence essential to predict CCN activity so that a quantitative  
6 assessment of atmospheric particles on cloud formation can be made. While numerous studies were  
7 performed to investigate the CCN activity under different atmospheric conditions around the world,  
8 only a few of them were made in the PRD region in China. In this study, several advanced instruments  
9 (i.e., the SMCA, AMS and H-TDMA) were used to respectively measure CCN activity, chemical  
10 composition, and hygroscopicity in PRD during wintertime 2014. Various schemes were proposed to  
11 determine the CCN activity based on the measurements. Here two important properties were  
12 considered when evaluating the CCN activity: the hygroscopic parameter  $\kappa$  and the surface tension of  
13 the particles. Three methods (i.e., the SMCA, the AMS+ZSR, and the H-TDMA) were employed to  
14 calculate the  $\kappa$  values based on our measurements. The results show that the deviation between  $\kappa_{\text{AMS}}$   
15 and  $\kappa_{\text{CCN}}$  became larger at low supersaturation ratios, indicating that aging process of organic  
16 component for larger size particles led to higher hygroscopicity for those particles. The activation curve  
17 became smoother at low SS, which could be partly attributed to the higher heterogeneity of chemical  
18 composition. In general, the Gf-PDF measured by H-TDMA exhibited a bimodal distribution with a  
19 less-hygroscopic mode and a more-hygroscopic mode. The less-hygroscopic mode was more  
20 significant at smaller diameters, indicating a more external mixing for smaller particles, while the  
21 more-hygroscopic increased with diameter and became broader, implying higher hygroscopicity and



1 more complex chemical composition for larger particles. The shape of activation curve was related to  
2 the  $\sigma$  values of the Gf-PDF. The higher  $\sigma$  values suggest the higher heterogeneity of chemical  
3 composition and smooth activation curve. A  $\kappa$  value of 0.22-0.30 measured by H-TDMA was obtained  
4 for 40-200 nm particles in this study during the measurement period, larger than those previously  
5 measured in the PRD region, which might indicate an increasing mass fraction of nitrate in recent  
6 years.

7  
8 Organic compounds could influence CCN activity through modifying the hygroscopicity and surface  
9 tension of the particles. The impacts of organics on CCN activity were also investigated in this study.  
10 The increase of organic mass fraction in the particles could lead to the decrease of the aerosol  
11 hygroscopicity and hence increase the  $D_{50}$ , especially at low supersaturation. In addition, organics  
12 could decrease the surface tension  $\sigma_{s/a}$ . This could lead to the underestimated CCN activity if pure  
13 water solution is assumed when inverting the H-TDMA data. We evaluated the impact of the surface  
14 tension on the activation ratios over a wide range of  $\sigma_{s/a}$  values ( $0.03$ - $0.07$  N m<sup>-1</sup>) for several measured  
15 size particles (40, 80, 110, and 150 nm) and found that a  $\sigma_{s/a}$  value of  $0.058$  N m<sup>-1</sup> was the best fit  
16 between predicted AR and measured AR, which could then be used to predict the CCN activity in the  
17 PRD region. Based on the hygroscopicity and chemical composition measured in this study, we  
18 proposed several scheme to predict the CCN activity. Overall, the predicted  $N_{CCN}$  agreed well with the  
19 measure one. The slope and  $R^2$  of  $N_{CCN}$  predicted from average data was similar to the  $N_{CCN}$  predicted  
20 from individual data. The  $N_{CCN}$  obtained from H-TDMA measurement was under-predicted, if pure  
21 water assumption was used and better agreement with the measured values can be achieved by using



1 the adjusted  $\sigma_{s/a}$  (i.e.,  $0.058 \text{ N m}^{-1}$ ). Similarly, the  $N_{\text{CCN}}$  predicted from AMS measurement was  
2 underestimated at low supersaturations and overestimated at high supersaturations, due to an  
3 assumption of fixed 0.1 for  $\kappa_{\text{org}}$  and the external mixing state. Better predicted CCN concentrations can  
4 be obtained by using  $\sigma_{s/a}^*$  and  $\kappa_{\text{org}}^*$  in the calculation, especially at low supersaturation. For high  
5 supersaturation, the effect of internal mixing assumption should be taken into consideration. We  
6 concluded that better CCN concentrations with the measurements could be achieved by taking the  
7 effects of organic into account on the hygroscopicity, surface tension, and the mixing state of the  
8 particles. More work on the roles of organics on the CCN activity is obviously needed in order to better  
9 understand the impacts of atmospheric particles on cloud formation and hence climate.

#### 10 **Acknowledgement**

11 The authors acknowledge the support from the following funding agencies: National Key R&D  
12 Program of China (2016YFC0201901, 2017YFC0209500, 2016YFC2003305), National Natural  
13 Science Foundation of China (NSFC) (91644225, 21577177, 41775117), and Guangdong provincial  
14 scientific planning project (2014A020216008, 2016B050502005). Support from the Science and  
15 Technology Innovative Research Team Plan of Guangdong Meteorological Bureau (Grant No.201704)  
16 is also acknowledged.

17

#### 18 **References**

19 Asaawuku, A., Engelhart, G. J., Lee, B. H., and Pandis, S. N.: Relating CCN activity, volatility, and  
20 droplet growth kinetics of  $\beta$ -caryophyllene secondary organic aerosol, Atmos. Chem. Phys., 9,  
21 795-812, 2009.



- 1 Cai, M., Tan, H., Chan, C. K., Mochida, M., Hatakeyama, S., Kondo, Y., Schurman, M. I., Xu, H., Li,  
2 F., Shimada, K., Liu, L., Deng, Y., Yai, H., Matsuki, A., Qin, Y., and Zhao, J.: Comparison of  
3 Aerosol Hygroscopicity, Volatility, and Chemical Composition between a Suburban Site in the Pearl  
4 River Delta Region and a Marine Site in Okinawa, *Aerosol Air Qual. Res.*, 17, 3194-3208, 2017.
- 5 Cao, G., Zhang, X., Wang, Y. and Zheng, F.: Estimation of emissions from field burning of crop straw  
6 in China, *Chin. Sci. Bull.*, 53, 784-790, 2008.
- 7 Cerully, K., Raatikainen, T., Lance, S., Tkacik, D., Tiitta, P., Petäjä, T., Ehn, M., Kulmala, M., Worsnop,  
8 D., and Laaksonen, A.: Aerosol hygroscopicity and CCN activation kinetics in a boreal forest  
9 environment during the 2007 EUCAARI campaign, *Atmos. Chem. Phys.*, 11, 12369-12386, 2011.
- 10 Chan, M. N., Kreidenweis, S. M., and Chan, C. K.: Measurements of the hygroscopic and  
11 deliquescence properties of organic compounds of different solubilities in water and their  
12 relationship with cloud condensation nuclei activities, *Environ. Sci. Technol.*, 42, 3602-3608, 2008.
- 13 Chang, R. Y. W., Slowik, J. G., Shantz, N. C., Vlasenko, A., Liggio, J., Sjostedt, S. J., Leitch, W. R.,  
14 and Abbatt, J. P. D.: The hygroscopicity parameter ( $\kappa$ ) of ambient organic aerosol at a field site  
15 subject to biogenic and anthropogenic influences: relationship to degree of aerosol oxidation,  
16 *Atmos. Chem. Phys.*, 10, 5047-5064, 2010.
- 17 Cheung H., Yeung M., Li Y., Lee B., and Chan C.: Relative Humidity-Dependent HTDMA  
18 Measurements of Ambient Aerosols at the HKUST Supersite in Hong Kong, China, *Aerosol Sci.*  
19 *Technol.*, 49, 643-654, 2015.
- 20 DeCarlo, P. F., Slowik, J. G., Worsnop, D. R., Davidovits, P., and Jimenez, J. L.: Particle Morphology  
21 and Density Characterization by Combined Mobility and Aerodynamic Diameter Measurements.



- 1 Part 1: Theory, *Aerosol Sci. Technol.*, 38, 1206-1222, 2004.
- 2 Decarlo, P. F., Kimmel, J. R., Achim, T., Northway, M. J., Jayne, J. T., Aiken, A. C., Marc, G., Katrin,  
3 F., Thomas, H., and Docherty, K. S.: Field-deployable, high-resolution, time-of-flight aerosol mass  
4 spectrometer, *Anal. Chem.*, 78, 8281-8289, 2006.
- 5 Deng, Z. Z., Zhao, C. S., Ma, N., Liu, P. F., Ran, L., Xu, W. Y., Chen, J., Liang, Z., Liang, S., Huang, M.  
6 Y., Ma, X. C., Zhang, Q., Quan, J. N., Yan, P., Henning, S., Mildenerger, K., Sommerhage, E.,  
7 Schäfer, M., Stratmann, F., and Wiedensohler, A.: Size-resolved and bulk activation properties of  
8 aerosols in the North China plain: the importance of aerosol size distribution in the prediction of  
9 CCN number concentration, *Atmos. Chem. Phys.*, 11, 3835-3846, 2011.
- 10 Engelhart, G., Asa-Awuku, A., Nenes, A., and Pandis, S.: CCN activity and droplet growth kinetics of  
11 fresh and aged monoterpene secondary organic aerosol, *Atmos. Chem. Phys.*, 8, 3937-3949, 2008.
- 12 Farmer, D. K., Cappa, C. D., and Kreidenweis, S. M.: Atmospheric Processes and Their Controlling  
13 Influence on Cloud Condensation Nuclei Activity, *Chem. Rev.*, 115, 4199-4217, 2015.
- 14 Good, N., Topping, D., Allan, J., Flynn, M., Fuentes, E., Irwin, M., Williams, P., Coe, H., and  
15 McFiggans, G.: Consistency between parameterisations of aerosol hygroscopicity and CCN activity  
16 during the RHaMBLe discovery cruise, *Atmos. Chem. Phys.*, 10, 3189-3203, 2010.
- 17 Gysel, M., Crosier, J., Topping, D. O., Whitehead, J. D., Bower, K. N., Cubison, M. J., Williams, P. I.,  
18 Flynn, M. J., McFiggans, G. B., and Coe, H.: Closure study between chemical composition and  
19 hygroscopic growth of aerosol particles during TORCH2, *Atmos. Chem. Phys.*, 7, 6131-6144, ,  
20 2007.
- 21 Gysel, M., McFiggans, G. B., and Coe, H.: Inversion of tandem differential mobility analyser (TDMA)



- 1        measurements, *J. Aerosol Sci.*, 40, 134-151, 2009.
- 2    Hong, J., Häkkinen, S. A. K., Paramonov, M., Äijälä, M., Hakala, J., Nieminen, T., Mikkilä, J., Prisle,  
3        N. L., Kulmala, M., and Riipinen, I.: Hygroscopicity, CCN and volatility properties of submicron  
4        atmospheric aerosol in a boreal forest environment during the summer of 2010, *Atmos. Chem.*  
5        *Phys.*, 14, 29097-29136, 2014.
- 6    Itahashi, S., Yumimoto, K., Uno, I., Hayami, H., Fujita, S., Pan, Y., and Wang, Y.: A 15-year record  
7        (2001–2015) of the ratio of nitrate to non-sea-salt sulfate in precipitation over East Asia, *Atmos.*  
8        *Chem. Phys.*, 18, 2835-2852, 2018.
- 9    Jiang, R., Tan, H., Tang, L., Cai, M., Yin, Y., Li, F., Liu, L., Xu, H., Chan, P. W., and Deng, X.:  
10       Comparison of aerosol hygroscopicity and mixing state between winter and summer seasons in  
11       Pearl River Delta region, China, *Atmos. Res.*, 169, 160-170, 2016.
- 12   Jimenez, J. L., Jayne, J. T., Shi, Q., Kolb, C. E., Worsnop, D. R., Yourshaw, I., Seinfeld, J. H., Flagan,  
13       R. C., Zhang, X., and Smith, K. A.: Ambient aerosol sampling using the aerodyne aerosol mass  
14       spectrometer, *J. Geophys. Res.: Atmos.*, 108, 8425, doi:10.1029/2001JD001213, 2003.
- 15   Köhler, H.: The nucleus in and the growth of hygroscopic droplets, *Trans. Faraday Soc.*, 32, 1152-1161,  
16       1936.
- 17   Lee, B. P., Li, Y. J., Yu, J. Z., Louie, P. K., and Chan, C. K.: Physical and chemical characterization of  
18       ambient aerosol by HR-ToF-AMS at a suburban site in Hong Kong during springtime 2011, *J.*  
19       *Geophys. Res.: Atmos.*, 118, 8625-8639, 2013.
- 20   Liu, H. J., Zhao, C. S., Nekat, B., Ma, N., Wiedensohler, A., van Pinxteren, D., Spindler, G., Müller, K.,  
21       and Herrmann, H.: Aerosol hygroscopicity derived from size-segregated chemical composition and



- 1 its parameterization in the North China Plain, Atmos. Chem. Phys., 14, 2525-2539, 2014.
- 2 Liu, P.F., Zhao, C.S., Göbel, T., Hallbauer, E., Nowak, A., Ran, L., Xu, W.Y., Deng, Z.Z., Ma, N.,
- 3 Mildenerger, K., Henning, S., Stratmann, F., and Wiedensohler, A., Hygroscopic properties of
- 4 aerosol particles at high relative humidity and their diurnal variations in the North China Plain.
- 5 Atmos. Chem. Phys., 11, 3479-3494, 2011
- 6 Meng, J. W., Yeung, M. C., Li, Y. J., Lee, B. Y. L., and Chan, C. K.: Size-resolved cloud condensation
- 7 nuclei (CCN) activity and closure analysis at the HKUST Supersite in Hong Kong, Atmos. Chem.
- 8 Phys., 14, 10267-10282, 2014.
- 9 Moore, R., Ingall, E., Sorooshian, A., and Nenes, A.: Molar mass, surface tension, and droplet growth
- 10 kinetics of marine organics from measurements of CCN activity, Geophys. Res. Lett., 35, L07801,
- 11 doi:10.1029/2008GL033350, 2008.
- 12 Moore, R., Bahreini, R., Brock, C., Froyd, K., Cozic, J., Holloway, J., Middlebrook, A., Murphy, D.,
- 13 and Nenes, A.: Hygroscopicity and composition of Alaskan Arctic CCN during April 2008, Atmos.
- 14 Chem. Phys., 11, 11807-11825, 2011.
- 15 Moore, R., Cerully, K., Bahreini, R., Brock, C., Middlebrook, A., and Nenes, A.: Hygroscopicity and
- 16 composition of California CCN during summer 2010, J. Geophys. Res.: Atmos., 117, D00V12,
- 17 doi:10.1029/2011JD017352, 2012.
- 18 Moore, R., Nenes, A., and Medina, J.: Scanning Mobility CCN Analysis—A Method for Fast
- 19 Measurements of Size-Resolved CCN Distributions and Activation Kinetics, Aerosol Sci. Technol.,
- 20 44, 861-871, 2010.
- 21 Ovadnevaite, J., Zuend, A., Laaksonen, A., Sanchez, K. J., Roberts, G., Ceburnis, D., Decesari, S.,



- 1 Rinaldi, M., Hodas, N., Facchini, M. C., Seinfeld, J. H., O'Dowd, C.: Surface tension prevails over  
2 solute effect in organic-influenced cloud droplet activation, *Nature*, 546, 637-641, 2017.
- 3 Pajunoja, A., Lambe, A. T., Hakala, J., Rastak, N., Cummings, M. J., Brogan, J. F., Hao, L., Paramonov,  
4 M., Hong, J., and Prisle, N. L.: Adsorptive uptake of water by semisolid secondary organic aerosols,  
5 *Geophys. Res. Lett.* 42, 3063-3068, 2015.
- 6 Petters, M., and Kreidenweis, S.: A single parameter representation of hygroscopic growth and cloud  
7 condensation nucleus activity, *Atmos. Chem. Phys.*, 7, 1961-1971, 2007.
- 8 Petters, M. D., and Kreidenweis, S. M.: A single parameter representation of hygroscopic growth and  
9 cloud condensation nucleus activity; Part 3: Including surfactant partitioning, *Atmos. Chem. Phys.*,  
10 13, 1081-1091, 2013.
- 11 Qin, Y. M., Tan, H. B., Li, Y. J., Schurman, M. I., Li, F., Canonaco, F., Prévôt, A. S. H., and Chan, C. K.:  
12 The role of traffic emissions in particulate organics and nitrate at a downwind site in the periphery  
13 of Guangzhou, China, *Atmos. Chem. Phys.*, 17, 1-31, 2017.
- 14 Rose, D., Nowak, A., Achtert, P., Wiedensohler, A., Hu, M., Shao, M., Zhang, Y., Andreae, M. O., and  
15 Pöschl, U.: Cloud condensation nuclei in polluted air and biomass burning smoke near the  
16 mega-city Guangzhou, China – Part 1: Size-resolved measurements and implications for the  
17 modeling of aerosol particle hygroscopicity and CCN activity, *Atmos. Chem. Phys.*, 10, 3365-3383,  
18 2010.
- 19 Sánchez Gácita, M., Longo, K. M., Freire, J. L., Freitas, S. R., and Martin, S. T.: Impact of mixing state  
20 and hygroscopicity on CCN activity of biomass burning aerosol in Amazonia, *Atmos. Chem. Phys.*,  
21 17, 2373-2392, 2017.



- 1 Salma, I., Ocskay, R., Varga, I., and Maenhaut, W.: Surface tension of atmospheric humic-like  
2 substances in connection with relaxation, dilution, and solution pH, *J. Geophys. Res.: Atmos.*, 111,  
3 D23205, [doi.org/10.1029/2005JD007015](https://doi.org/10.1029/2005JD007015), 2006.
- 4 Schurman, M. I., Kim, J. Y., Cheung, H. H. Y., and Chan, C. K.: Atmospheric particle  
5 composition-hygroscopic growth measurements using an in-series hybrid tandem differential  
6 mobility analyzer and aerosol mass spectrometer, *Aerosol Sci. Technol.*, 51, 694-703, 2017.
- 7 Sjogren, S., Gysel, M., Weingartner, E., Alfarra, M.R., Duplissy, J., Cozic, J., Crosier, J., Coe, H., and  
8 Baltensperger, U.: Hygroscopicity of the submicrometer aerosol at the high-alpine site Jungfraujoch,  
9 3580 m a.s.l., Switzerland, *Atmos. Chem. Phys.* 8, 5715-5729, 2008.
- 10 Sorjamaa, R., Svenningsson, B., Raatikainen, T., Henning, S., Bilde, M., and Laaksonen, A.: The role  
11 of surfactants in Köhler theory reconsidered, *Atmos. Chem. Phys.*, 4, 2107-2117, 2004.
- 12 Stocker, D. Q.: Climate change 2013: The physical science basis, Working Group I Contribution to the  
13 Fifth Assessment Report of the Intergovernmental Panel on Climate Change, Summary for  
14 Policymakers, IPCC, 2013.
- 15 Stokes, R., and Robinson, R.: Interactions in aqueous nonelectrolyte solutions. I. Solute-solvent  
16 equilibria, *J. Phys. Chem.*, 70, 2126-2131, 1966.
- 17 Stolzenburg, M. R., and McMurry, P. H.: Equations Governing Single and Tandem DMA  
18 Configurations and a New Lognormal Approximation to the Transfer Function, *Aerosol Sci.*  
19 *Technol.*, 42, 421-432, 2008.
- 20 Tan, H., Xu, H., Wan, Q., Li, F., Deng, X., Chan, P. W., Xia, D., and Yin, Y.: Design and Application of  
21 an Unattended Multifunctional H-TDMA System, *J. Atmos. Ocean. Technol.*, 30, 1136-1148, 2013.



- 1 Tan, H., Yin, Y., Li, F., Liu, X., Chan, P.W., Deng, T., Deng, X., Wan, Q. and Wu, D.: Measurements of  
2 particle number size distributions and new particle formation events during winter in the pearl river  
3 delta region, China, *J. Trop. Meteor.*, 22, 191-199, 2016.
- 4 Topping, D. O., McFiggans, G. B., and Coe, H.: A curved multi-component aerosol hygroscopicity  
5 model framework: Part 1 – Inorganic compounds, *Atmos. Chem. Phys.*, 5, 1205-1222, 2005.
- 6 Tritscher, T., Dommen, J., Decarlo, P. F., and Gysel, M.: Volatility and hygroscopicity of aging  
7 secondary organic aerosol in a smog chamber, *Atmos. Chem. Phys.*, 11, 11477-11496, 2011.
- 8 Väisänen, O., Ruuskanen, A., Ylisirniö, A., Miettinen, P., Portin, H., Hao, L., Leskinen, A., Komppula,  
9 M., Romakkaniemi, S., and Lehtinen, K. E. J.: In-cloud measurements highlight the role of aerosol  
10 hygroscopicity in cloud droplet formation, *Atmos. Chem. Phys.*, 16, 1-24, 2016.
- 11 Wang, J., Cubison, M., Aiken, A., Jimenez, J., and Collins, D.: The importance of aerosol mixing state  
12 and size-resolved composition on CCN concentration and the variation of the importance with  
13 atmospheric aging of aerosols, *Atmos. Chem. Phys.*, 10, 7267-7283, 2010.
- 14 Wu, Z. J., Poulain, L., Henning, S., Dieckmann, K., Birmili, W., Merkel, M., van Pinxteren, D.,  
15 Spindler, G., Müller, K., Stratmann, F., Herrmann, H., and Wiedensohler, A.: Relating particle  
16 hygroscopicity and CCN activity to chemical composition during the HCCT-2010 field campaign,  
17 *Atmos. Chem. Phys.*, 13, 7983-7996, 2013.
- 18 Zdanovskii, A.: New methods for calculating solubilities of electrolytes in multicomponent systems,  
19 *Zhur. Fiz. Khim.*, 22, 1475–1485, 1948.
- 20 Zhang, X. Y., Wang, J. Z., Wang, Y. Q., Liu, H. L., Sun, J. Y., and Zhang, Y. M.: Changes in chemical  
21 components of aerosol particles in different haze regions in China from 2006 to 2013 and



1 contribution of meteorological factors, Atmos. Chem. Phys., 15, 12935-12952, 2015.

2



1 **Table 1.** The  $\kappa$  values of the related species in the study.

Species	$\kappa$
NH <sub>4</sub> NO <sub>3</sub>	0.58
NH <sub>4</sub> HSO <sub>4</sub>	0.56
H <sub>2</sub> SO <sub>4</sub>	0.90
(NH <sub>4</sub> ) <sub>2</sub> SO <sub>4</sub>	0.48
Organics	0.10

2



1 **Table 2.** Summary of the measured CCN concentration, activation ratio, and  $D_{50}$  at the four  
2 supersaturations during the campaign.

SS		0.1%	0.2%	0.4%	0.7%
	Max	15165	19989	25964	26208
$N_{CCN}(\#/cm^3)$	Min	258	361	408	502
	Mean±STD	3103±1913	5095±2972	6524±3783	7913±4234
	Max	0.68	0.75	0.89	0.94
Activation	Min	0.06	0.10	0.19	0.28
Ratio	Mean±STD	0.26±0.10	0.41±0.14	0.53±0.15	0.64±0.13
	Max	268.90	194.04	145.28	97.17
$D_{50}$ (nm)	Min	112.47	76.60	43.50	24.21
	Mean±STD	156.02±19.48	106.66±16.99	77.96±14.86	58.45±10.68

3



1 **Table 3.** The average  $\sigma$  values of Gf-PDF measured by H-TDMA for the five diameters at four  
2 supersaturations. At each SS, the  $\sigma$  values are respectively calculated for the steep and smooth  
3 activation.

SS(%)	0.1		0.2		0.4		0.7	
Dp(nm)	Steep	Smooth	Steep	Smooth	Steep	Smooth	Steep	Smooth
40	0.13	0.17	0.12	0.17	0.11	0.19	0.11	0.19
80	0.16	0.20	0.14	0.20	0.14	0.21	0.14	0.20
110	0.17	0.21	0.15	0.21	0.15	0.21	0.16	0.20
150	0.19	0.22	0.17	0.23	0.17	0.22	0.18	0.21
200	0.20	0.23	0.19	0.24	0.19	0.24	0.19	0.23

4



1 **Table 4.** The schemes used in the  $N_{CCN}$  prediction based on H-TDMA measurement.

Scheme	Method	Slope	$R^2$
1	Real time activation curve	0.8275	0.93
2	Average activation curve	0.8183	0.93
3	Real time $D_{50}$	0.8869	0.93
4	Average $D_{50}$	0.8738	0.93
5	Real time activation curve using $\sigma_{s/a}^*$	0.9377	0.93

2



1 **Table 5.** The methods used in the  $N_{CCN}$  prediction based on AMS measurement.

Scheme	Method	Slope	$R^2$
6	Real time bulk composition	0.9859	0.91
7	Average bulk composition	1.0108	0.91
8	Real time size-resolved composition	0.9721	0.87
9	Average size-resolved composition	0.9742	0.86

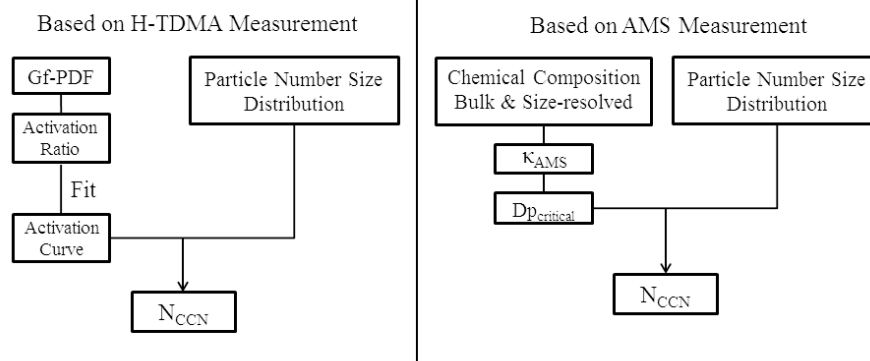
2



- 1    FIGURE CAPTIONS
- 2    Fig. 1. A schematic representation of  $N_{CCN}$  prediction based on H-TDMA and AMS measurements.
- 3    Fig. 2. The mass fraction of the bulk NR- $PM_{10}$  composition (a) and the mass fraction of the
- 4    size-resolved composition (b).
- 5    Fig. 3. The median and interquartile PNSD and the corresponding  $\kappa$  values obtained from H-TDMA,
- 6    AMS, and CCN measurement during the campaign. The  $\kappa$  was plotted against their corresponding
- 7    median  $D_{50}$  (SMCA and AMS) or measured diameter (H-TDMA). Dot points represent the median
- 8    value and the bars represent the interquartile range. The blue, red, and green represent  $\kappa_{CCN}$ ,  $\kappa_{AMS}$ , and
- 9     $\kappa_{H-TDMA}$  respectively.
- 10   Fig. 4. The sized resolved activation ratios measured by SMCA at the four different supersaturations.
- 11   Fig. 5. The Gf-PDF as a function of Gf measured by H-TDMA for the five particle diameters (40, 80,
- 12   110, 150, 200 nm)
- 13   Fig. 6. The relationship between size-resolved mass fraction of organics and  $D_{50}$  at the three
- 14   supersaturations. The red, blue, and green dots and line represent 0.1%, 0.2%, and 0.4% SS
- 15   respectively.
- 16   Fig. 7. The predicted activation ratio based on H-TDMA measurement vs. the measured activation ratio
- 17   at 0.1%, 0.2%, 0.4% and 0.7% SS for 40, 80, 110, 150 and 200 nm particles. The pure water for surface
- 18   tension ( $0.072 \text{ N m}^{-1}$ ) was assumed when calculating the AR.
- 19   Fig. 8. The relative deviation between predicted AR and measured AR at different assumed  $\sigma_{s/a}$ . The
- 20   color code represents  $R^2$  between calculated AR and measured AR.
- 21   Fig. 9. The predicted activation ratio using new surface tension assumption ( $\sigma_{s/a}^*$ ) based on H-TDMA
- 22   measurement vs. the measured activation ratio at 0.1%, 0.2%, 0.4% and 0.7% SS for 40, 80, 110, 150



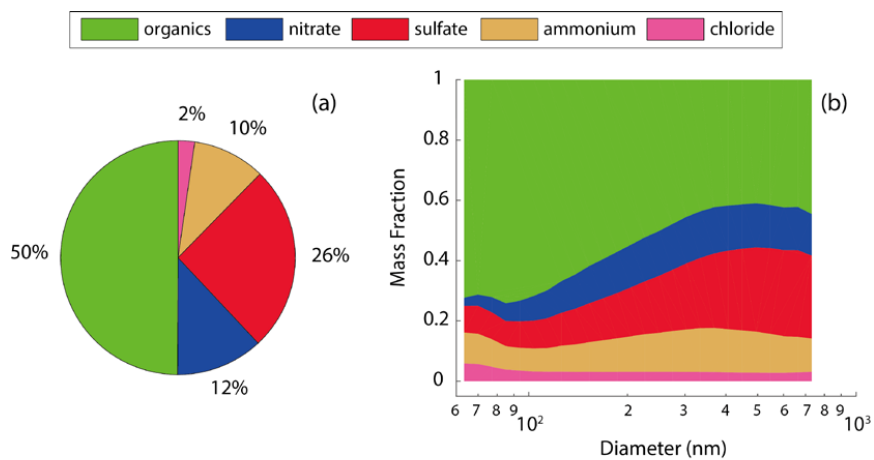
- 1 and 200 nm particles.
- 2 Fig. 10. The relationship between measured  $N_{CCN}$  and predicted  $N_{CCN}$  based on scheme 1, 2, 3, 4 and 5.
- 3 Fig. 11. The relationship between measured  $N_{CCN}$  and predicted  $N_{CCN}$  based on scheme 6, 7, 8 and 9.
- 4 Fig. 12. The relationship between measured  $N_{CCN}$  and predicted  $N_{CCN}$  at SS 0.1% based on
- 5 size-resolved chemical composition using  $\kappa_{org}^*$  (a), and  $\kappa_{org}^*$  and  $\sigma_{s/a}^*$  (b). The shadow area represents
- 6 the variation of the linear fit using the  $\sigma_{s/a}$  values between 0.054 and 0.062  $N\ m^{-1}$ .



1  
2  
3 Fig. 1.



1



2

3

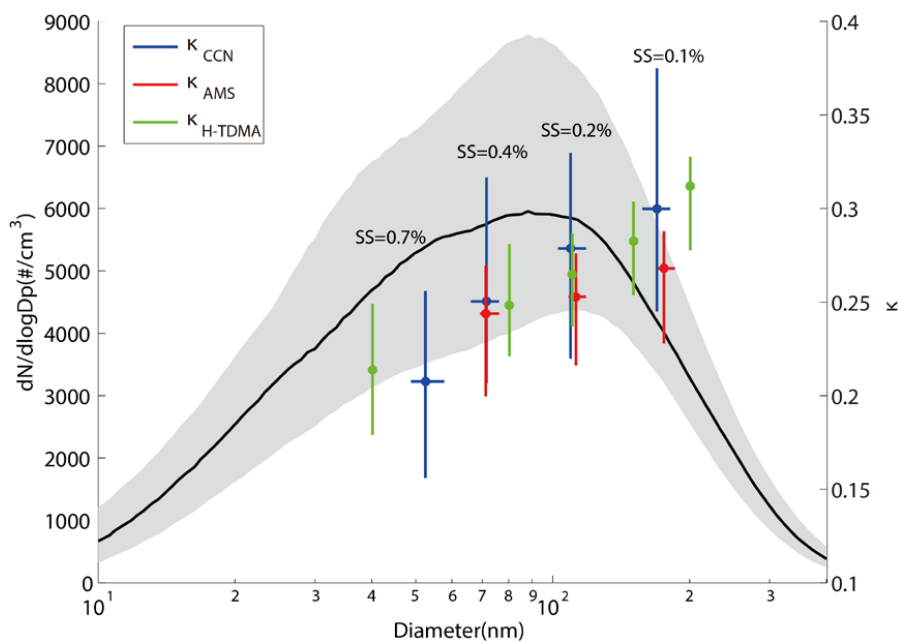
4 Fig. 2.

5

6



1



2

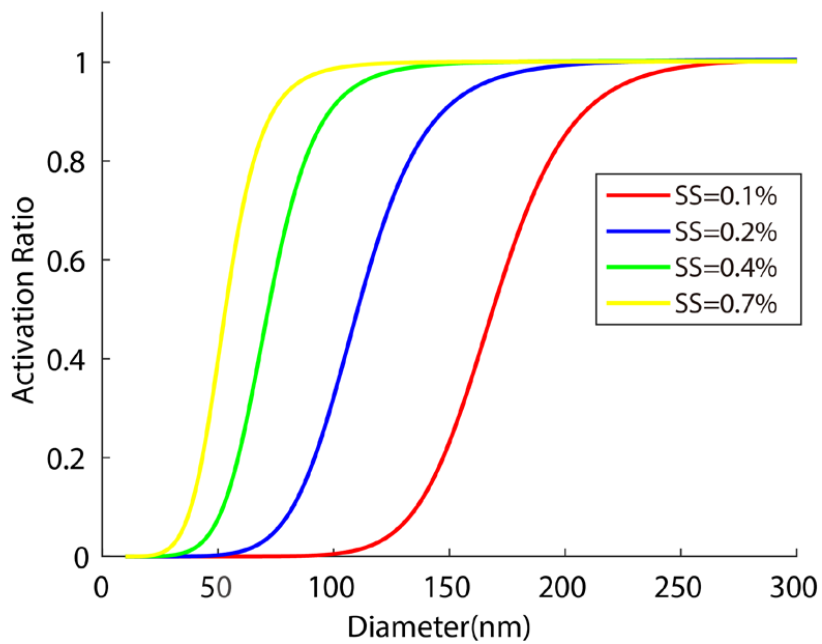
3 Fig. 3.

4

5



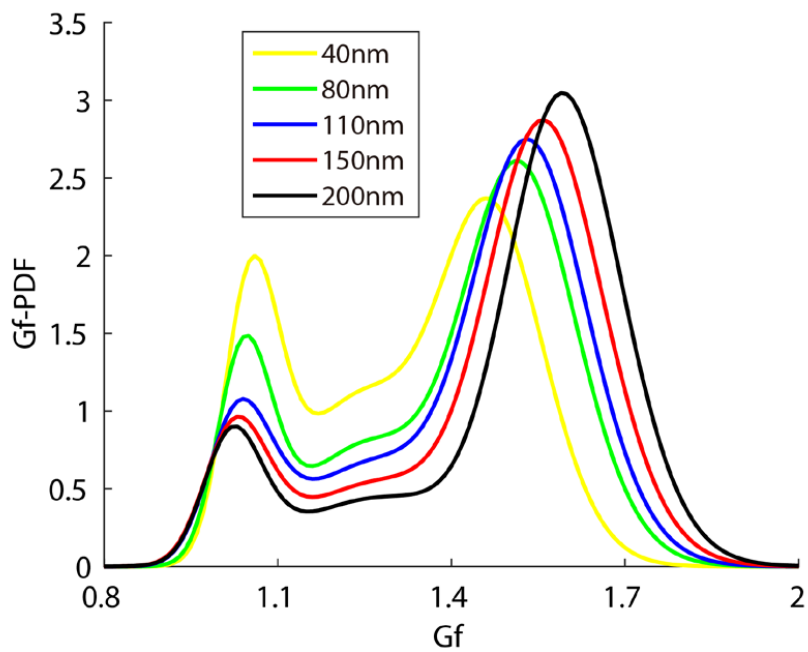
1



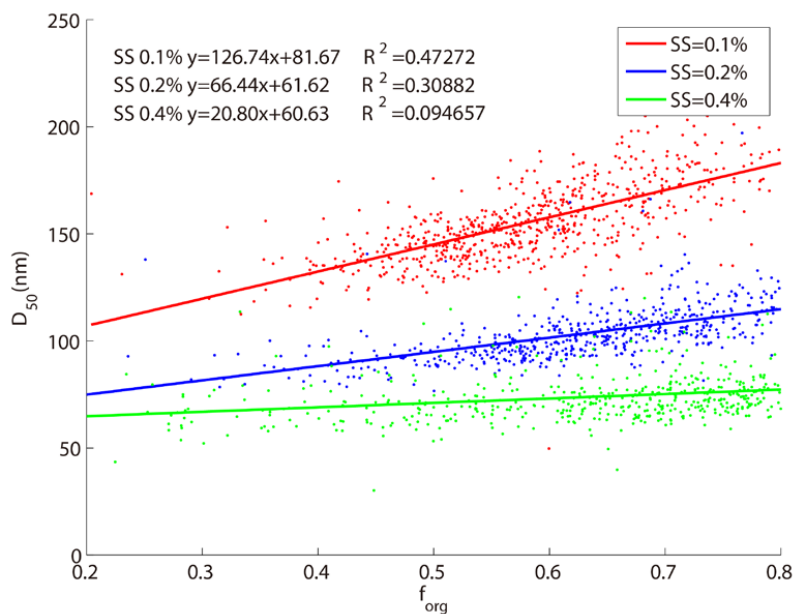
2

3 Fig. 4.

4



1  
2  
3 Fig. 5.  
4  
5



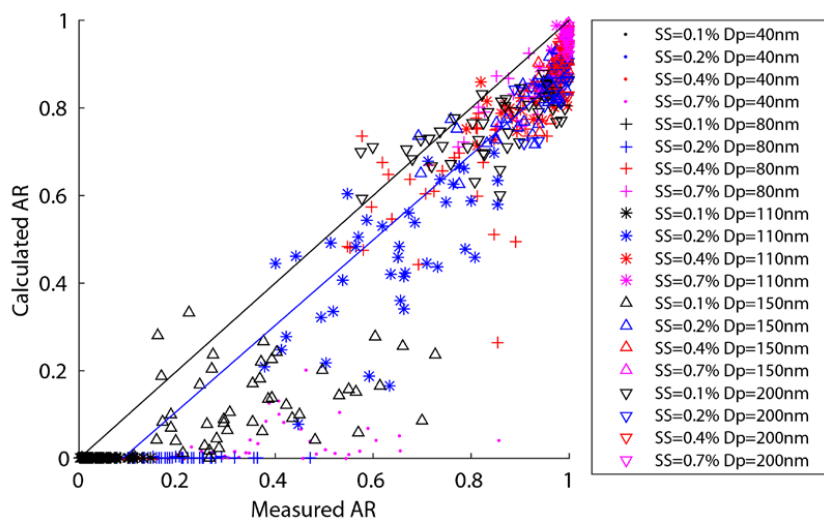
1

2 Fig. 6.

3



1



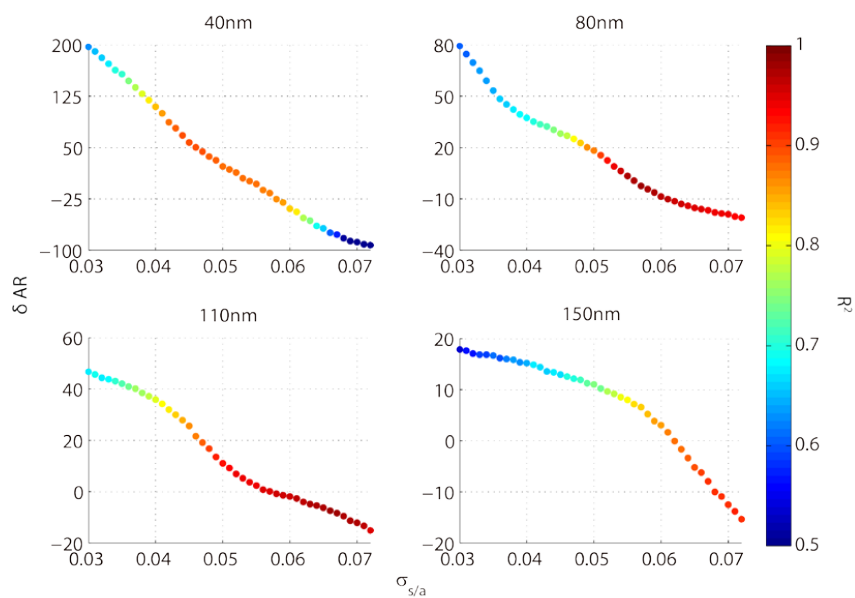
2

3 Fig. 7.

4



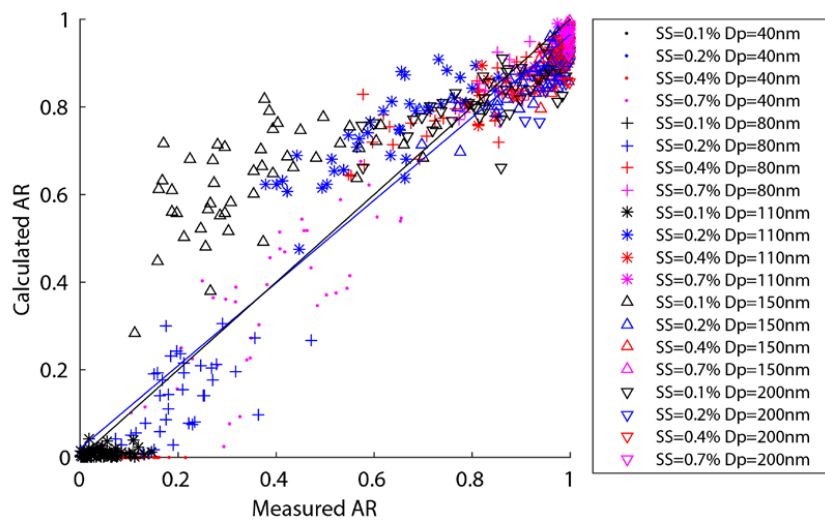
1



2

3 Fig. 8.

4

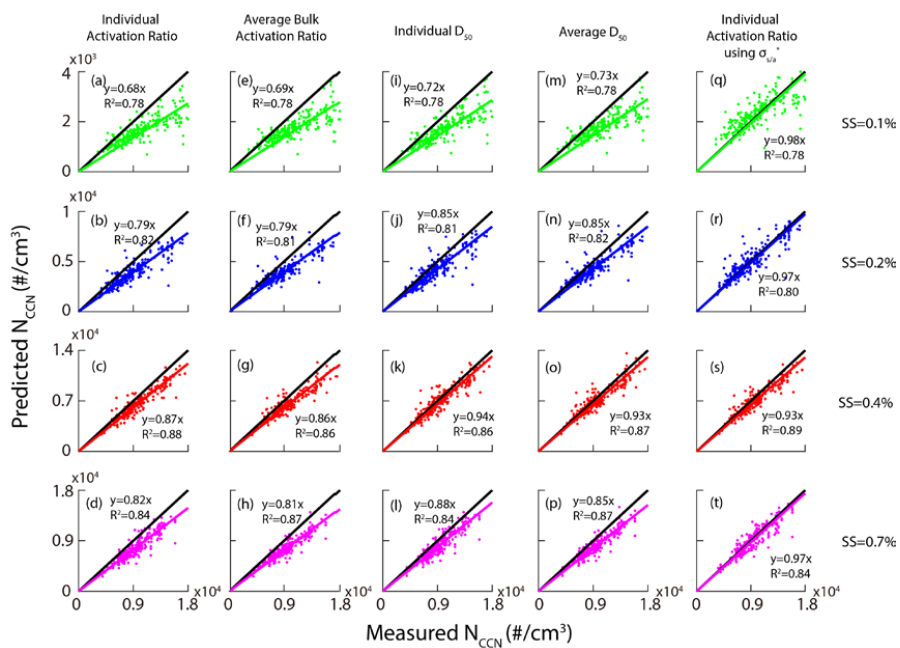


1

2

3 Fig. 9.

4

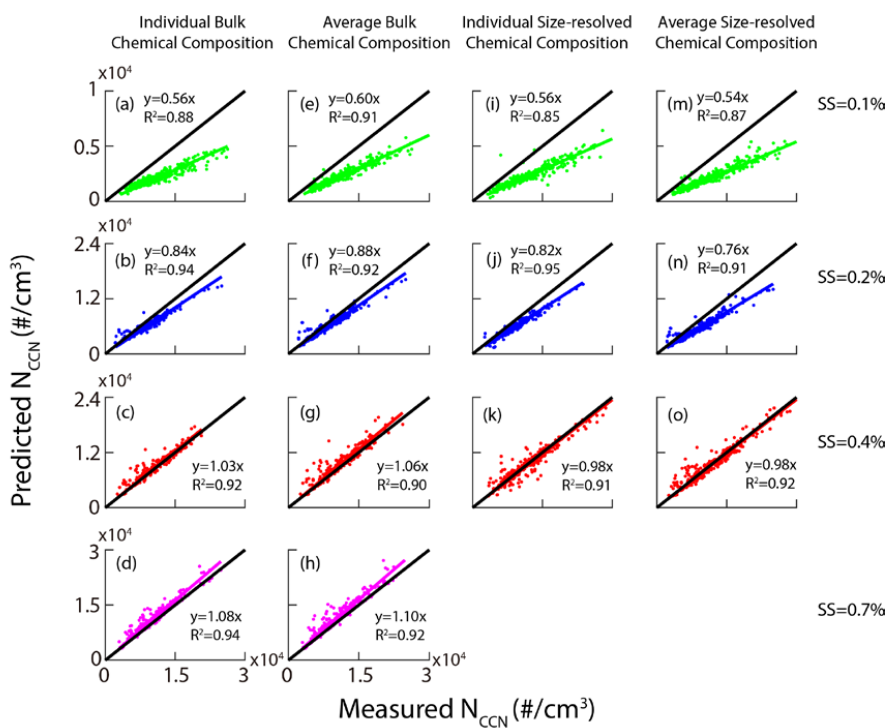


1

2

3 Fig. 10.

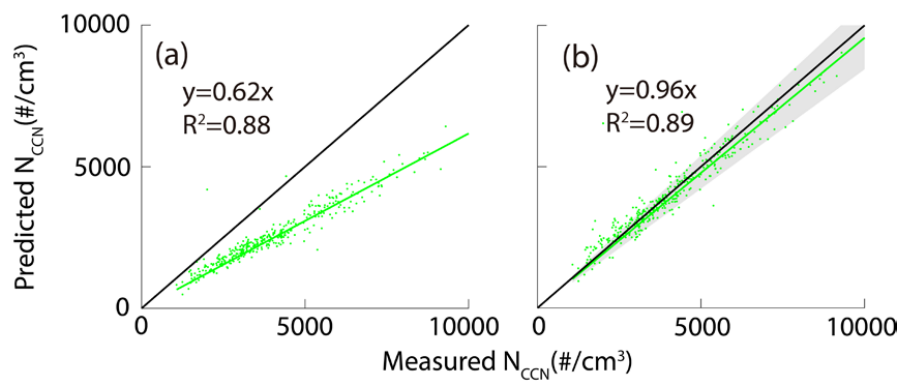
4



1

2 Fig. 11.

3



1

2

3 Fig. 12.